Reliable Viscosity from Equilibrium Molecular Dynamics Simulations: A Time Decomposition Method

Yong Zhang, Akihito Otani and Edward J. Maginn*

Department of Chemical and Biomolecular Engineering

University of Notre Dame

Notre Dame, Indiana, 46556 USA

March 10, 2015

*Corresponding author. E-mail: ed@nd.edu

Abstract

A viscosity calculation method based on Green-Kubo relation and equilibrium molecular dynamics simulation was proposed. In this method, instead of one long trajectory usually used in such calculation, multiple trajectories are generated. The Green-Kubo relation is applied to each trajectory, the averaged running integral as a function of time is fitted to a double exponential function with the weighting function derived from the standard deviation of the running integrals. Such a weighting function guarantees the accuracy of the fit even at long times, avoids the well known long time tail problem. In practice, however, to save computational time, short correlation time is preferred and a cutoff time t_{cut} is suggested, which can be determined by the relative values of the running integral and the corresponding standard deviation. All simulation parameters can be determined by following objective standards, guarantees the results to be reliable and reproducible. The method was demonstrated by applying to relative low viscosity liquid ethanol and relatively high viscosity ionic liquid 1-n-butyl-3-methylimidazolium bis(trifluoromethane-sulfonyl)imide ($[BMIM][Tf_2N]$), and found to be robust.

Keywords: Green-Kubo, Ionic Liquids, standard deviation, system size effect

1 Introduction

Viscosity is one of the most essential physical properties of a liquid in industrial applications. In addition to experimental studies,[1–5] different theoretical methods including equilibrium and non-equilibrium molecular dynamics (MD) methods have been developed to understand and predict viscosities.[2,6–16] Due to its simplicity, the Green-Kubo relation based on equilibrium MD simulations has been a popular method.

In the Green-Kubo relation, the shear viscosity can be calculated from the integral over time of the pressure tensor autocorrelation function[17]

$$\eta = \frac{V}{k_B T} \int_0^\infty \langle P_{\alpha\beta}(t) \cdot P_{\alpha\beta}(0) \rangle \, dt \tag{1}$$

where V is the system volume, k_B is the Boltzmann constant, T is temperature, $P_{\alpha\beta}$ denotes the element $\alpha\beta$ of the pressure tensor. Theoretically, the pressure tensor autocorrelation function decays to zero at long time limit and the integration reaches a constant, which corresponds to the calculated shear viscosity. In practice, however, due to the well known long time tail in such correlation function,[18] the integration does not converge to a constant and usually include large errors at long times. A calculation example is shown in Figure 1, in which the running integrals using eq 1 are calculated from three independent trajectories generated for ethanol at 298 K. Each trajectory is 10 nanosecond (ns) long. It can be seen that the three curves start to deviate in less than 100 picosecond (ps) and reach dramatically different values at 1 ns.

The statistics in eq 1 can be improved by taking averages over the six independent pressure tensor.[19,20] The curves shown in Figure 1 considered such average already. Not like self-diffusivity or other dynamic properties, viscosity is a collective property, the statistics can not be improved by averaging over number of particles. A very long trajectory is needed for good statistics. Equivalently, an alternative strategy is to run multiple independent trajectories and take the average,[21,22] which benefits from the available massive parallel computation facilities and save wall time. In Figure 1, the average of the three individual curves are also provided and it is smoother than the individual ones, especially at short

times.

Due to the long time tail, the viscosity is usually determined from a short time "plateau" region. However, the identify of the plateau region can be arbitrary. Sometimes, it is even hard to identify such a region. For the curve calculated from one trajectory (traj 1) shown in Figure 1, the region between 100 $\sim$ 200 ps might be a plateau region, the region around 300 ps can be another option. It is even harder to define the plateau region in the other two curves. Once a plateau is somehow identified, it is still not clear how to derive the viscosity from this region. Different procedures have been reported in the literature. One way is to take the value at a chosen cutoff time. Zhang and Nie[23] set the cutoff to the time when the autocorrelation function first reaches zero in their study of liquid iron. Similar idea was also used in an earlier work by Alfe and Gillan[24] in the study of liquid aluminum and iron-sulfur alloy. However, it has been pointed out that such a definition of cutoff time can be misleading because the zero crossing time is mainly the result of statistical fluctuations and depends a lot on the calculation details.[21] In the study of liquid tin, Gasser and coworkers applied a cutoff time of 2ps without rationalization. A much longer cutoff time, up to 5 ns, was applied by Mondal and Balasubramanian in their recent study of ionic liquid (IL) systems,[22] which seems to be longest possible time from their correlation function. Instead of taking a value at certain point, a probably better alternative is to take the average value over a region in the running integral.[25,26] However, all these procedures are somewhat arbitrary and the results from different procedures can be quite different.

A more systematic way to obtain viscosity from Green-Kubo relation is to fit either the pressure tensor autocorrelation function or the running integral in eq 1 to a function and derive the viscosity at long time limit analytically. The Kohlrausch law has been used to fit the autocorrelation function.[27,28] To fit the running integral, the double exponential function of the form

$$\eta(t) = A\alpha\tau_1(1 - e^{-t/\tau_1}) + A(1-\alpha)\tau_2(1 - e^{-t/\tau_2}) \tag{2}$$

has been suggested where A, α, τ_1 *and* τ_2 are fitting parameters.[20,29] To reduce the noise at long times, Rey-Castro and Vega applied a weighting factor of $1/t^2$ in the fitting.[29]

In spite of these development, reliable calculation of viscosity is still a challenging task, partly due to the arbitrariness in the procedure and the lack of an objective way to setup the simulation, especially for high viscosity liquid where statistics is usually poor within accessible simulation time scale. ILs are examples of such liquids. ILs are defined as salts with melting points below 100 °C. Due to their unique properties such as low vapor pressure, large liquid phase range and nonflamibility, ILs promises various applications in industry. However, ILs are usually more viscous than traditional molecular solvent by 1-2 orders, which means augmented cost in transport and limits their usage as solvents.

In the current work, we introduce a time-decomposition method for the reliable calculation of shear viscosity from equilibrium MD simulation. The detailed procedure is provided and it is expected that if the same procedure is properly followed, the results can be easily reproduced and results from different people are directly comparable. The procedure was demonstrated by applying to a low viscosity molecular solvent ethanol and relatively high viscosity IL, 1-n-butyl-3-methylimidazolium bis(trifluoromethane-sulfonyl)imide ($[BMIM][Tf_2N]$).

2 Simulation Procedure and Details

2.1 Molecular Dynamics Simulation

Equilibrium MD simulations were carried out using the LAMMPS package.[30] For both ethanol and $[BMIM][Tf_2N]$, the general Amber force field (GAFF)[31] was used to describe the inter- and intramolecular interactions. To derive the partial charges, the structure of the ethanol molecule or each isolated ion in $[BMIM][Tf_2N]$ was optimized at the B3LYP/6-311++g(d,p) level using the Gaussian 09 package.[32] The atomic charges were then derived by fitting the electrostatic potential surface using the RESP method.[33] The charges obtained this way are directly used for ethanol. For $[BMIM][Tf_2N]$, the charges were uniformly scaled by 0.8 to account for the effect of charge transfer and polarizability.[34] The long range electrostatic interactions were calculated using the particle-particle particle-mesh

(PPPM) method[35] with real space cutoff of 12 Å. For all simulations, a time step of 1 femtosecond (fs) was used and the periodic boundary conditions were applied in all directions. The simulation box was built up by putting molecules randomly in a cubic box using the package Packmol.[36,37] The ethanol box contains 1000 molecules and the $[BMIM][Tf_2N]$ system contains 300 ion pairs, respectively. The systems were then equilibrated for 2ns in the isothermal-isobaric (NPT) ensemble followed by canonical (NVT) ensemble production runs. The pressure tensor were saved every 5 fs during the NVT simulation. The Nosé-Hoover thermostat[38] and the extended Lagrangian approach[39] were applied to control the temperature and pressure, respectively. Simulations were carried out at five temperatures (283, 298, 303, 323, and 343 K, respectively) for ethanol and four temperatures (350, 400, 450 and 500 K, respectively) for $[BMIM][Tf_2N]$. The pressure was fixed to be one atmosphere in all constant pressure simulations with isotropic volume fluctuations.

2.2 Time-Decomposition Method of Viscosity

The shear viscosity was calculated by following procedure.

(1) Generate N independent NVT trajectories at a given temperature;

(2) For each trajectory, calculate the shear viscosity based on Green-Kubo relation (eq 1);

(3) Calculate the average of the running integrals over N trajectories and the standard deviation, which is a function of time:

$$\sigma(t) = \sqrt{\frac{1}{N-1}\sum_{i=1}^{N}(\eta(t)_i - \langle\eta(t)\rangle)^2} \tag{3}$$

(4) Fit the standard deviation to a power function

$$\sigma(t) = At^b \tag{4}$$

(5) Fit the averaged running integral by the double exponential function (eq 2) for the time period up to t_{cut} with the weight $1/t^b$, where b is the fitting result from step (4) and t_{cut} can be decided from the relation between η and $\sigma(t)$. We found that the time when $\sigma(t)$

is about 40% of the average η is a good choice. Take the long time limit of the fitted double exponential function as the calculated viscosity;

(6) Increase N and repeat steps (1)-(5) till the change in the calculated viscosity in step (5) from previous cycle is smaller than a tolerance.

Details of this time-decomposition procedure is described in the next section.

3 Results and Discussions

Based on the results of the NPT ensemble simulations, the density as a function of temperature was calculated for each system. The results are shown in Figure 2 and compared with experimental values. For ethanol, the calculated densities were found to be about 2.5% higher than experimental results. For $[BMIM][Tf_2N]$, simulations were carried out at relatively high temperatures for faster dynamics and better sampling. The calculated densities at high temperatures were fitted to a linear function and extrapolated to low temperatures. As shown in the figure, the agreement with experimental results are almost perfect. For both ethanol and $[BMIM][Tf_2N]$, small deviations can be seen between the experimental results. Overall, however, the calculated densities agree with experimental results very well, which is a sign that the applied force fields can describe the systems reasonably well.

3.1 Viscosity of Ethanol

3.1.1 Weighting Function

In order to calculate the viscosity, 100 independent trajectories were generated starting from the same configuration but a different random seed for initial velocity assignment. Each trajectory is 5 ns long. The first ns of each trajectory was considered equilibration and ignored in the viscosity calculation. Based on each trajectory, the shear viscosity was calculated based on eq 1 and the average at each temperature is provided in Figure 3 (top panel). Different from the noisy curves in Figure 1, the averages are much better behaved. In each case, following a sharp increase in short time, the running integral reaches a flat

region. However, even with the average of 100 independent trajectories, the random error in the correlation function is not fully canceled out and the curves are not completely flat, especially at long times. The standard deviation based on eq 3 are calculated and provided in Figure 3 (bottom panel). As expected, the standard deviation increase as the time becomes longer due to the long time tail in the correlation function.[18] At each temperature, the standard deviation can be fit to a power function $\sigma(t) = At^b$ (eq 4) where t is time, A and b are fitting parameters.

In order to derive viscosity, the averaged running integral was fitted to the double exponential function (eq 2).[29] Different from $1/t^2$ used by Rey-Castro and coworkers,[29] the fitting results of the standard deviation $1/t^b$ was used as weighting function in the fit. With this weighting function, the short time data points that have higher accuracy have more weight in the fitting and the less accurate data points at long times have less weight, similar idea applied by Rey-Castro and coworkers.[29] However, we realized that $1/t^2$ weight decays too fast so that for systems with high viscosity, the weight becomes negligible before reaching the plateau region and significantly underestimate the viscosity. Figure 4 shows such an example. On the other hand, the relatively mild weighting function used here works fine even in very high viscosity cases and the way the weighting function is determined guarantees that each data point used in the fit contribute the same error to final results even long time data points are included.

3.1.2 Cutoff Time t_{cut}

In practice, however, fitting to relatively short period of time is still preferred for the sake of reducing computational cost. Therefore, a parameter t_{cut} is introduced to characterize the upper time limit that the fit is applied to. It is found that the time at which the calculated standard deviation $\sigma(t)$ has the value about 40% of the corresponding viscosity (rough average of the flat region in the running integral) is a good choice for t_{cut}. For example, for the results shown in Figure 3 (top panel), at 298 K, the flat region of the running integral has a value around 1.3 cP, 40% of which is about 0.52 cP, which corresponds to a

$t_{cut} = 700ps$ based on the σ values shown in Figure 3 (lower panel). During the fitting, it was found that the running integral fluctuates a lot at very short time due to the fast decay of the correlation function, as shown in Figure 5. Because of the large weight of this period of time, such fluctuation makes the fitting unstable. Therefore, the first 2ps of the running integral is ignored in the fitting. With these considerations, Figure 6 shows the fitting results of ethanol at 298 K. The calculated standard deviation and the corresponding fitting results is provided as inset. The b parameter was found to have a value of 0.52, which is close to the observation by Danel, Kazandjian and Zerah,[26] who reported that the calculated standard deviation varies roughly like $\sqrt{t}$. Based on the double exponential fitting to the running integral with weight of $1/t^{0.52}$, the viscosity was found to be 1.318 cP, which is close to experimental values $\sim$ 1.1 cP.[40–45] It is worth mentioning that for ethanol at 298 K, the t_{cut} value can be as short as 200 ps, where σ has the value about 20% of viscosity. In this case, the calculated viscosity was found to be 1.312 cP. With both t_{cut}, the viscosities are within 2% deviation from the results with t_{cut} = 2000 ps, which is the maximum possible time with enough accuracy from the 4ns trajectory and corresponds to σ value of 70% of the calculated viscosity. These results agree with the fact that the applied weighting function properly minimizes the error even when more noisy long time region is included in the fitting.

The viscosities at other temperatures were derived by following the same procedure and the results are shown in Figure 7 (top panel) and compared with available experimental values. There are small deviations in the experimental values, but overall, the agreement between the calculated and experimentally measured viscosities is very well especially considering that viscosity is usually a very hard property to calculate. At each temperature, the b parameters were found to be between 0.41-0.56. For comparison, the weighting function $1/t^{0.5}$ was also used to all temperatures and the calculated viscosities agree with those using $1/t^b$ very well as shown in the lower panel in Figure 7.

3.1.3 Number of Trajectories

Above discussion is based on 100 independent trajectories to demonstrate the general calculation procedure. Actually, fewer trajectories would be enough to obtain the results and the nice thing about the proposed procedure is, as described in the previous section, that one can always start with a few trajectories and add more when it is necessary until the results are converged. The top left panel in Figure 8 shows the cumulative average of up to 100 trajectories. The top right panel in the figure shows the corresponding standard deviation. The calculated standard deviation at four time points are explicitly provided in the lower left panel of the figure. As shown in the plots, both the averaged running integral and standard deviation converged with about 30-40 trajectories. Following the procedure described above, the viscosities as a function of number of trajectories were derived and provided in the lower right panel of Figure 8. With 40 or more trajectories, the calculated viscosities were found to be less than 1% away from each other, indicating the convergence of the simulation. The results with $1/t^{0.5}$ weight were also provided for comparison, which agree with $1/t^{b}$ weighting function results almost perfectly.

3.1.4 Trajectory Length

Not only the number of trajectories can be smaller, the length of each trajectory can also be shorter. Using only the last 500 ps, 1 ns or 2 ns from the 5 ns trajectories at 298 K, the viscosities were calculated and the results are shown in Figure 9 and compared with results using 4 ns trajectories. As expected, the calculated standard deviation becomes larger when shorter trajectories are used. Using the same criteria that the viscosity is about 40% of standard deviation, the cutoff time t_{cut} was found to be 400 ps when 2 ns trajectories were used, 200 ps when 1 ns trajectories were used, and 90 ps when 500 ps trajectories were used, respectively. Using either 1 or 2 ns trajectories, as shown in the lower panel of Figure 9, the calculated viscosities still converge with 40 trajectories although the fluctuations are larger than the results when 4 ns trajectories were used (but still within 1-2% from each other). In either case, the results are within 2-3% deviation from those using 4 ns trajectories. It

is interesting to note that the results from 1 ns trajectories are lower than 4 ns trajectories results whereas results from 2 ns trajectories are higher then 4 ns trajectories results. The randomness of the deviation indicates that even 1 ns trajectories are long enough in this case. However, with only 500 ps trajectories, the running integral does not really reach a flat region (top panel). The calculated viscosities do not seem converge either even with 100 trajectories, indicating that 500 ps is too short for the calculation of reliable viscosity in this case.

3.1.5 System Size Effect

The effect of simulation system size is also studied. In addition to the 1000 ethanol molecule box, a smaller box with 500 molecules and a bigger box with 1500 molecules were setup and simulations were carried out following the same procedure. The calculated running integral and standard deviation from 100 trajectories are shown in Figure 10. Both pressure and viscosity are collective properties. As the result, the accuracy can not be improved by increasing the system size. As shown in the plots, the calculated standard deviation are almost the same for the three systems with different sizes. The derived viscosities are also very similar, within 1% from each other, consistent with previous reports.[9,24,46]

3.2 Viscosity of $[BMIM][Tf_2N]$

The same procedure was applied to $[BMIM][Tf_2N]$, which has much higher viscosity than ethanol at room temperature. To accelerate the dynamics, the simulations were carried out at high temperatures between 350 and 500 K with 50 K interval. Like the case of ethanol, 100 independent trajectories were generated at each temperature, each is 7 ns long at 350 K and 5 ns long at other temperatures. The first 1 ns was ignored in each trajectory and the pressure tensor auto-correlation function was calculated based on the rest. The averaged running integral and the corresponding standard deviation at each temperature are shown in Figure 11. The standard deviation were fit to power function $\sigma(t) = At^b$ and the parameters b were found to have values between 0.60-0.73, slightly higher than those of ethanol. Again,

the cutoff time t_{cut} was determined by taking the time at which the calculated standard deviation is about 40% of the viscosity value at each temperature. The t_{cut} was found to be 1100, 800, 800 and 700 ps at 350, 400, 450 and 500 K, respectively. Lower than 40% could be used at each temperatures as long as the results does not change much. For example, at 350 K, with 30% cutoff, t_{cut} was found to be 800 ps and the calculated viscosity is only 0.8% lower. But if 20% is used, the calculated viscosity becomes 6.1% lower. For liquids with lower viscosity such as ethanol discussed above or $[BMIM][Tf_2N]$ at higher temperature, lower than 30% could be used as well. For liquids with even higher viscosity, it was found that 40% is still a good option (results not shown here) so it is consistently used in the current work. Similar to ethanol, large fluctuation was found in the first 2 ps of the running integral (as shown in the bottom panel in Figure 11) so the first 2 ps was ignored in the fitting.

The calculated viscosities for $[BMIM][Tf_2N]$ as a function of temperature are shown in Figure 12. To compare with the experimental results at relatively low temperature, the calculated viscosities were fitted to the Arrhenius equation

$$\eta = \eta_0 exp(E/(RT)) \tag{5}$$

and the Vogel-Tamman-Fulcher (VTF) equation,[47] respectively,

$$\eta = Aexp(B/(T - T_0)) \tag{6}$$

and extrapolated to experimental temperatures. In above equations, η_0, E, A, B and T_0 are fitting parameters and R is ideal gas molar constant. As shown in Figure 12 (upper panel), using both equations, the extrapolated viscosities are systematically higher than experimental results.[48–53] At high temperatures, the results from both Arrhenius and VTF equations are similar and about twice of those from experiments. At low temperatures, the deviation from experiments becomes smaller and Arrhenius equation results behaves slightly better than VTF equation, deviation as small as 20% is observed at 283 K.

The correlation coefficients of the fitting are 0.9998 for Arrhenius equation and 0.9999 for VTF equation, respectively, suggesting reliable fits in both cases. However, because there are

only four data points to fit two (Arrhenius) or three (VTF) parameters in the equations, not mentioning the uncertainty in the calculated results, it is very likely that the extrapolated results include large uncertainty. So in addition to extrapolate the calculated viscosity to experimental temperatures, the experimental data were also fit to above equations (or directly taken from literature when available[48,49,51,52]) and extrapolated to simulational temperature range. The results are shown in the lower panel in Figure 12. In this case, the results from VTF equation are clearly better than those from Arrhenius equation. Overlap between calculated and extrapolated experimental results are observed at high temperature, where the simulational results are likely more accurate. Overall, the simulated viscosities agree reasonably well with experimental measurements.

Similar to the case of ethanol, more than enough trajectories (both number and length of trajectories) were generated to demonstrate the viscosity calculation of $[BMIM][Tf_2N]$. Figure 13 shows the calculated viscosities of $[BMIM][Tf_2N]$ as a function of trajectory numbers at 350 K. With 30 or more trajectories, the calculated viscosity are about 2-3% deviation from each other, slightly larger than the case in ethanol. For comparison, the weighting function $1/t^{0.5}$ was also applied and the results are shown in the same plot. The results using $1/t^{0.5}$ as weighting function are systematically higher than the results using $1/t^b$ by 2-3%. This difference is large relative to the almost perfect agreement in the case of ethanol, likely due to the larger b parameters derived for $[BMIM][Tf_2N]$. However, considering the deviation from experimental results, these differences are negligible. At least for test runs before the simulation conditions are optimized, $1/t^{0.5}$ weighting function can be used.

4 Concluding Remarks

Equilibrium MD simulation is still a popular technique for the calculation of viscosity due to its simplicity and the fact that the generated trajectories can also be used to derive other system properties, an advantage over non-equilibrium MD methods. However, the

method based on Green-Kubo relation has arbitrariness, therefore the calculated results can be unreliable and difficult to reproduce. In the current work, a time-decomposition method was proposed for the calculation of viscosity using the Green-Kubo relation based on equilibrium MD simulations. Great details were provided with the hope to setup a objective and standard procedure so that the results can be easily judged and reproduced.

The proposed method decomposes one long equilibrium MD trajectory into multiple independent short ones. The Green-Kubo relation is applied to each of such short trajectories and the averaged running integral is used to derive the viscosity. The standard deviation in the individual running integrals is also calculated and fitted to a power function, which is used as weighting function in the fit to the double exponential function of the averaged running integral. The standard deviation is also used to decide the time range (characterized by t_{cut}) during which the running integral is fitted. The necessary number of independent trajectories and the length of each trajectory can be easily decided with a few test runs. By applying the procedure to ethanol and $[BMIM][Tf_2N]$, the calculated results are found not sensitive to the choice of simulation conditions, indicating the robustness of the procedure. It is worth mentioning that, because each trajectory is independent of each other, the statistic accuracy of the proposed procedure can be further improved by applying mathematic tricks such as bootstrap method.[54]

For the two examples discussed in the current work, the calculated viscosities agree with experimental measurement reasonably well although a general purpose force field (GAFF) was used in the simulation. However, it should be understood that the focus in the current work is to demonstrate the viscosity simulation procedure rather than to show the accurate results for a few examples. Therefore, it is more interesting to compare the calculated results with different options. With the proposed procedure, the simulation results are likely further improved if a dedicated force field is used.[46,55]

Acknowledgment

This material is based upon work supported by the U.S. Department of Energy, Basic

Energy Science, Joint Center for Energy Storage Research under Contract No. DE-AC02-06CH11357. Computational resources were provided by the National Energy Research Scientific Computing Center, which is supported by the Office of Science of the U.S. Department of Energy under Contract No. DE-AC02-05CH11231, and the Center for Research Computing (CRC) at the University of Notre Dame.

References

[1] Gurkan, B.; Goodrich, B. F.; Mindrup, E. M.; Ficke, L. E.; Massel, M.; Seo, S.; Senftle, T. P.; Wu, H.; Glaser, M. F.; Shah, J. K.; Maginn, E. J.; Brennecke, J. F.; Schneider, W. F. Molecular Design of High Capacity, Low Viscosity, Chemically Tunable Ionic Liquids for CO(2) Capture. *J. Phys. Chem. Lett.* **2010,** *1,* 3494-3499.

[2] Atilhan, M.; Jacquemin, J.; Rooney, D.; Khraisheh, M.; Aparicio, S. Viscous behavior of imidazolium-based ionic liquids. *Ind. Eng. Chem. Res.* **2013,** *52,* 16774-16785.

[3] Blahusiak, M.; Schlosser, S. Physical properties of phosphonium ionic liquid and its mixtures with dodecane and water. *J. Chem. Thermodynamics* **2014,** *72,* 54-64.

[4] Prabhu, S. R.; Dutt, G. B. Rotational dynamics of imidazolium-based ionic liquids: Do the nature of the anion and the length of the alkyl chain influence the dynamics? *J. Phys. Chem. B* **2014,** *118,* 13244-13251.

[5] Ren, Z.; Ivanova, A. S.; Couchot-Vore, D.; Garrett-Roe, S. Ultrafast Structure and Dynamics in Ionic Liquids: 2D-IR Spectroscopy Probes the Molecular Origin of Viscosity. *J. Phys. Chem. Lett.* **2014,** *5,* 1541-1546.

[6] Cummings, P. T.; Evans, D. J. Nonequilibrium molecular dynamics approaches to transport properties and non-newtonian fluid rheology. *Ind. Eng. Chem. Res.* **1992,** *31,* 1237-1252.

[7] Hu, Z.; Margulis, C. J. Room-temperature ionic liquids: slow dynamics, viscosity, and the red edge effect. *Acc. Chem. Res.* **2007,** *40,* 1097-1105.

[8] Wang, X.; Chi, Y.; Mu, T. A review on the transport properties of ionic liquids. *J. Mol. Liq.* **2014,** *193,* 262-266.

[9] Yeh, I.; Hummer, G. System-size dependence of diffusion coefficients and viscosities from molecular dynamics simulations with periodic boundary condictions. *J. Phys. Chem. B* **2004,** *108,* 15873-15879.

[10] Hu, Z.; Margulis, C. J. On the response of an ionic liquid to external perturbations and the calculationof shear viscosity. *J. Phys. Chem. B* **2007,** *111,* 4705-4714.

[11] Kelkar, M. S.; Maginn, E. J. Effect of temperature and water content on the shear viscosity of the ionic liquid 1-ethyl-3-methylimidazolium bis(trifluoromethanesulfonly)imide as studied by atomistic simulations. *J. Phys. Chem. B* **2007,** *111,* 4867-4876.

[12] Borodin, O.; Smith, G. D.; Kim, H. Viscosity of a room temperature ionic liquid: predictions from nonequilibrium and equilibrium molecular dynamics simulations. *J. Phys. Chem. B* **2009,** *113,* 4771-4774.

[13] Reyes, G.; Segura, H.; Mejia, A. Coarse-grained molecular dynamic simulations of selected thermophysical properties for 1-butyl-3-methylimidazolium hexafluorophosphate. *J. Mol. Liq.* **2013,** *186,* 106-115.

[14] Llovell, F.; Marcos, R. M.; Vega, L. F. Free-volume theory coupled with soft-SAFT for viscosity calculations: Comparison with molecular simulation and experimental data. *J. Phys. Chem. B* **2013,** *117,* 8159-8171.

[15] Chen, Z.; Lee, J.-m. Free volume model for the unexpected effect of C2-mythylation on the properties of imidazolium ionic liquids. *J. Phys. Chem. B* **2014,** *118,* 2712-2718.

[16] Choi, E.; McDaniel, J. G.; Schmidt, J. R.; Yethiraj, A. First-principles, physically motivated force field for the ionic liquid [BMIM][BF4]. *J. Phys. Chem. Lett.* **2014,** *5,* 2670-2674.

[17] Allen, M. P. *Computer Simulation of Liquids;* Oxford University Press: 1987.

[18] Levesque, D.; Verlet, L. Computer experiments on classical fluids. IV. Transport properties and time-correlation functions of the Lennard-Jones liquid near its triple point. *Phys. Rev. A* **1973,** *7,* 1690-1700.

[19] Daivis, P. J.; Evans, D. J. Comparison of constant pressure and constant volume nonequilibrium simulations of sheared model decane. *J. Chem. Phys.* **1994,** *100,* 541-547.

[20] Hess, B. Determining the shear viscosity of model liquids from molecular dynamics simulations. *J. Chem. Phys.* **2002,** *116,* 209-217.

[21] Mouas, M.; Gasser, J.-G.; Hellal, S.; Grosdidlier, B.; Makradi, A.; Belouettar, S. Diffusion and viscosity of liquid tin: Green-Kubo relationship-based calculations from molecular dynamics simulations. *J. Chem. Phys.* **2012,** *136,* 094501.

[22] Mondal, A.; Balasubramanian, S. A molecular dynamics study of collective transport properties of imidazolium-based room-temperature ionic liquids. *J. Chem. Eng. Data* **2014,** *59,* 3061-3068.

[23] Zhang, Y.; Guo, G.; Nie, G. A molecular dynamics study of bulk and shear viscosity of liquid iron using embedded-atom potential. *Phys. Chem. Minerals* **2000,** *27,* 164-169.

[24] Alfe, D.; Gillan, M. J. First-principles calculation of transport coefficients. *Phys. Rev. Lett.* **1998,** *81,* 5161-5164.

[25] Chen, T.; Smit, B.; Bell, A. T. Are pressure fluctuation-based equilibrium methods really worse than nonequilibrium methods for calculating viscositues? *J. Chem. Phys.* **2009,** *131,* 246101.

[26] Danel, J. F.; Kazandjian, L.; Zerah, G. Numerical convergence of the self-diffusion coefficient and viscosity obtained with Thomas-Fermi-Dirac molecular dynamics. *Phys. Rev. E* **2012,** *85,* 066701.

[27] Guo, G.; Zhang, Y.; Refson, K.; Zhao, Y. Viscosity and stress autocorrelation function in supercooled water: a molecular dynamics study. *Mol. Phys.* **2002,** *100,* 2617-2627.

[28] Meyer, E. R.; Kress, J. D.; Collins, L. A.; Ticknor, C. Effect of correlation on viscosity and diffusion in molecular-dynamics simulations. *Phys. Rev. E* **2014,** *90,* 043101.

[29] Rey-Castro, C.; Vega, L. F. Transport Properties of Ionic Liquid 1-ethyl-3-methylimidazolium Chloride from Equilibrium Molecular Dynamics Simulation. The Effect of Temperature. *J. Phys. Chem. B* **2006,** *110,* 14426-14435.

[30] Plimpton, S. Fast Parallel Algorithms for Short-range Molecular Dynamics. *J. Comp. Phys.* **1995,** *117,* 1-19.

[31] Wang, J.; Wolf, R. M.; Caldwell, J. W.; Kollman, P. A.; Case, D. A. Development and Testing of a General Amber Force Field. *J. Comput. Chem.* **2004,** *25,* 1157-1174.

[32] Frisch, M. J. *et al.* "Gaussian 09 Revision A.1", Gaussian Inc. Wallingford CT 2009.

[33] Bayly, C.; Cieplak, P.; Cornell, W. D.; Kollman, P. A. A Well-behaved Electrostatic Potential Based Method Using Charge Restraints for Deriving Atomic Charges: the RESP Model. *J. Phys. Chem.* **1993,** *97,* 10269-10280.

[34] Zhang, Y.; Maginn, E. J. A Simple AIMD Approach to Derive Atomic Charges for Condensed Phase Simulation of Ionic Liquids. *J. Phys. Chem. B* **2012,** *116,* 10036-10048.

[35] Hockney, R.; Eastwood, J. *Computer simulation using particles;* Adam Hilger, New York: 1989.

[36] Martinez, J. M.; Martinez, L. Packing Optimization for Automated Generation of Complex System's Initial Configurations for Molecular Dynamics and Docking. *J. Comput. Chem.* **2003,** *24,* 819-825.

[37] Martinez, L.; Andrade, R.; Martinez, J. M. Software News and Update Packmol: A Package for Building Initial Configurations for Molecular Dynamics Simulations. *J. Comput. Chem.* **2009,** *30,* 2157-2164.

[38] Hoover, W. G. Canonical dynamics: Equilibrium phase-space distributions. *Phys. Rev. A* **1985,** *31,* 1695-1697.

[39] Shinoda, W.; Shiga, M.; Mikami, M. Rapid estimation of elastic constants by molecular dynamics simulation under constant stress. *Phys. Rev. B* **2004,** *69,* 134103.

[40] Khattab, I. S.; Bandarkar, F.; Fakhree, M. A. A.; Jouyban, A. Density, viscosity, and surface tension of water+ethanol mixtures from 293 to 323 K. *Korean J. Chem. Eng.* **2012,** *29,* 812-817.

[41] Nain, A. K. Ultrasonic and viscometric studies of molecular interactions in binary mixtures of formamide with ethanol, 1-propanol, 1,2-ethanediol and 1,2-propanediol at different temperatures. *J. Mol. Liq.* **2008,** *140,* 108-116.

[42] Bhuiyan, M. M. H.; Uddin, M. H. Excess molar volumes and excess viscosities for mixtures of N,N-dimythylformamide with methanol, ethanol and 2-propanol at different temperatures. *J. Mol. Liq.* **2008,** *138,* 139-146.

[43] Pires, R. M.; Costa, H. F.; Ferreira, A. G. M.; Fonseca, I. M. A. Viscosity and density of water + ethyl acetate + ethanol mixtures at 298.15 and 318.15 K and atmospheric pressure. *J. Chem. Eng. Data* **2007,** *52,* 1240-1245.

[44] Alvarez, E.; Cancela, A.; Maceiras, R.; Navaza, J. M.; Taboas, R. Density, viscosity, excess molar volume, and viscosity deviation of three amyl alcohols + ethanol binary mixtures from 293.15 to 323.15 K. *J. Chem. Eng. Data* **2006,** *51,* 940-945.

[45] Gonzalez, B.; Dominguez, A.; Tojo, J. Dynamic viscosities, densities, and speed of sound and derived properties of the binary systems acetic acid with water, methanol, ethanol, ethyl acetate and methyl acetate at T=(293.15, 298.15, and 303.15) K at atomospheric pressure. *J. Chem. Eng. Data* **2004,** *49,* 1590-1596.

[46] Andreussi, O.; Marzari, N. Transprot properties of room-temperature ionic liquids from classical molecular dynamics. *J. Chem. Phys.* **2012,** *137,* 044508.

[47] Fulcher, G. S. Analysis of recent measurements of the viscosity of glasses. *J. Am. Ceram. Soc.* **1925,** *8,* 339-355.

[48] Vranes, M.; Dozic, S.; Djeric, V.; Gadzuric, S. Physicochemical characterization of 1-butyl-3-methylimidazolium and 1-butyl-1-methylpyrrolidinium bis(trifluoromethylsulfonyl)imide. *J. Chem. Eng. Data* **2012,** *57,* 1072-1077.

[49] Tatsuta, S.; Shiozawa, Y.; Imai, K.; Kudo, Y.; Takeda, Y. Stability of ion pairs of bis(trifluoromethanesulfonyl)amide-based ionic liquids in dichloromethane. *J. Chem. Eng. Data* **2010,** *55,* 1588-1593.

[50] Tokuda, H.; Tsuzuki, S.; Susan, M. A. B. H.; Hayamizu, K.; Matanabe, M. How ionic are room-temperature ionic liquids? An indicator of the physicochemical properties. *J. Phys. Chem. B* **2006,** *110,* 19593-19600.

[51] Jacquemin, J.; Husson, P.; Padua, A. A. H.; Majer, V. Density and viscosity of several pure and water-saturated ionic liquids. *Green Chem.* **2006,** *8,* 172-180.

[52] Tokuda, H.; Hayamizu, K.; Ishii, K.; Susan, M. A. B. H.; Watanabe, M. Physicochemical Properties and Structures of Room Temperature Ionic Liquids. 2. Variation of Alkyl Chain Length in Imidazolium Cation. *J. Phys. Chem. B* **2005,** *109,* 6103-6110.

[53] Okoturo, O. O.; VanderNoot, T. J. Temperature dependence of viscosity for room temperature ionic liquids. *J. Electroana. Chem.* **2004,** *568,* 167-181.

[54] Chernick, M. R. *Bootstrap methods a guide for practitioners and researchers;* John Wiley and Sons, Inc., Hoboken, New Jersey: 2008.

[55] Voroshylova, I. V.; Chaban, V. V. Atomistic force field for pyridinium-based ionic liquids: Reliable transprot properties. *J. Phys. Chem. B* **2014,** *118,* 10716-10724.

[56] Wandschneider, A.; Lehmann, J. K.; Heintz, A. Surface tension and density of pure ionic liquids and some binary mixtures with 1-propanol and 1-butanol. *J. Chem. Eng. Data* **2008,** *53,* 596-599.

[57] Jacquemin, J.; Husson, P.; Mayer, V.; Cibulka, I. High-pressure volumetric properties of imidazolium-based ionic liquids: effect of the anion. *J. Chem. Eng. Data* **2007,** *52,* 2204-2211.

Figure captions

Figure 1. Example results of viscosity calculations using the Green-Kubo relation based on three independent 10 ns trajectories generated for ethanol at 298 K. Due to the well known long time tail in the pressure autocorrelation function, the three running integrals deviate in less than 100 ps and end up at significantly different values at 1 ns, which makes it very difficult to derive a reliable viscosity from such calculation. The average of the three running integral is also provided in the plot, which is much smoother than each individual one.

Figure 2. Calculated densities as function of temperature and compared with experimental results. Upper panel: ethanol, experimental results: Exp. a, ref;[40] Exp. b, ref;[42] Exp. c, ref;[43] Exp. d, ref;[44] Exp. e, ref.[45] Lower panel: $[BMIM][Tf_2N]$, experimental results: Exp. a, ref;[48] Exp. b, ref;[49] Exp. c, ref;[50] Exp. d, ref;[51] Exp. e, ref;[56] Exp. f, ref.[57] The calculated densities at high temperature were fitted to a linear function and extrapolated to lower experimental temperature range (shown as dotted line). For both ethanol and $[BMIM][Tf_2N]$, the calculated densities agree with experimental results very well.

Figure 3. The calculated averaged running integral (eq 1) and standard deviation (eq 3) from 100 independent 5 ns long equilibrium MD trajectories for ethanol at different temperatures.

Figure 4. Example results of fitting the running integral to the double exponential function (eq 2) with a $1/t^2$ weight. The running integral is averaged over 100 independent trajectories generated for $[BMIM][Tf_2N]$ at 350 K, each trajectory is 7 ns long. The weighting function decays too fast and the fitting result significantly underestimates the contribution from long time scales. A weighting function of the form $1/t^b$ is suggested in this work, where b is derived by fitting the calculated standard deviation to a power function $\sigma(t) = Ae^b$, which was found to work well even for high viscosity liquid.

Figure 5. The large fluctuation at very short time in the calculated running integral of ethanol. Each curve is an average over 100 independent ones. The same fluctuation is

also seen in each individual curve (not shown). This fluctuation behavior makes the fitting unstable due to the heavy weight in this time range. The first 2 ps of the running integral was therefore ignored in the fitting.

Figure 6. The fitting results of the averaged running integral to the double exponential function (eq 2) with $1/t^b$ weight. The inset shows the fitting results of the calculated standard deviation to the power function $\sigma(t) = Ae^b$. The parameter t_{cut} was found to be 700 ps in this case which is the time at which the calculated standard deviation has the value of around 40% of the viscosity (as shown by the flat region in the running integral). The parameter b was found to be 0.52. Results at other temperatures show similar behavior.

Figure 7. Upper panel: The calculated viscosity of ethanol using the proposed time-decomposition method and compared with experimental results. The agreement with experimental results are reasonably well. Experimental results: Exp. a, ref;[40] Exp. b, ref;[41] Exp. c, ref;[42] Exp. d, ref;[43] Exp. e, ref;[44] Exp. f, ref.[45] Lower panel: Comparison of the calculated viscosities with $t_{cut} = 700ps$ and $t_{cut} = 2000ps$. Because of the average over multiple independent trajectories and the use of proper weighting function, the results are not sensitive to the t_{cut} value. However, short t_{cut} is preferred to save simulational time.

Figure 8. The effect of number of independent trajectories on the calculated viscosity. Results are shown for ethanol at 298 K, behavior at other temperatures are similar. Upper left: the cumulative average of the running integral; upper right: the calculated standard deviation for corresponding cumulative average (same color code); lower left: the calculated standard deviation as a function of the number of independent trajectories at several time points; lower right: calculated viscosity as a function of the number of independent trajectories, the results with $1/t^{0.5}$ weight was also provided for comparison. All plots shown that the results converge with 40 or more independent trajectories.

Figure 9. The effect of length of each independent trajectory on the calculated viscosity. Upper panel: the averaged running integral (over 100 independent trajectories) and the corresponding standard deviation; lower panel: the calculated viscosity as a function of the number of independent trajectories. When 4, 2 or 1 ns trajectories were used, the calculated

results are close to each other and all converge with 40 trajectories although slightly larger fluctuations are seen when short trajectories were used. When 500 ps trajectories were used, the results show relatively large deviations from other results, indicating the trajectories are probably too short.

Figure 10. The effect of simulation system size on the calculated viscosity. Systems containing 500, 1000 or 1500 ethanol molecules are used in the simulation. Results are averages over 100 independent trajectories in each case. The results show that, because pressure and viscosity are collective properties, the calculated running integral and the corresponding standard deviation are independent of the system size. The calculated viscosities are within 1% deviation from each other.

Figure 11. The calculated results using the time-decomposition method for $[BMIM][Tf_2N]$ at different temperatures. All results are based on 100 independent trajectories. Top panel: the calculated averaged running integral (eq 1); middle panel: the calculated standard deviation (eq 3); bottom panel: the large fluctuation in the very short time region in the averaged running integral, the same as the case in ethanol.

Figure 12. The calculated viscosity of $[BMIM][Tf_2N]$ using the proposed time-decomposition method and compared with experimental results. Upper panel: the calculated viscosities at high temperature were fitted to VTF or Arrhenius equations and extrapolated to low experimental temperatures. Due to the limited number of calculated viscosities and the uncertainty in the results, the extrapolated results likely include relatively large errors. Lower panel: the experimental results were fitted to VTF or Arrhenius equations and extrapolated to higher temperatures. The results using VTF equation is better than those using Arrhenius equation. Better agreement between calculated and experimental results are seen. Overall, the calculated viscosity agree with experimental results reasonably well. Experimental results: Exp. a, ref;[48] Exp. b, ref;[49] Exp. c, ref;[50] Exp. d, ref;[51] Exp. e, ref;[52] Exp. f, ref.[53]

Figure 13. The effect of number of independent trajectories on the calculated viscosity. Results are shown for $[BMIM][Tf_2N]$ at 350 K, behavior at other temperatures are similar. The calculated viscosity converged with about 30 or more independent trajectories. The

results with $1/t^{0.5}$ weight were also provided for comparison. Different from the almost exact agreement in the case of ethanol, the difference between results with two weighting functions are slightly larger in this case (but still $< 3\%$), likely due to the fact that the b parameters have values between 0.60-0.73 whereas the b parameters are close 0.5 for ethanol.

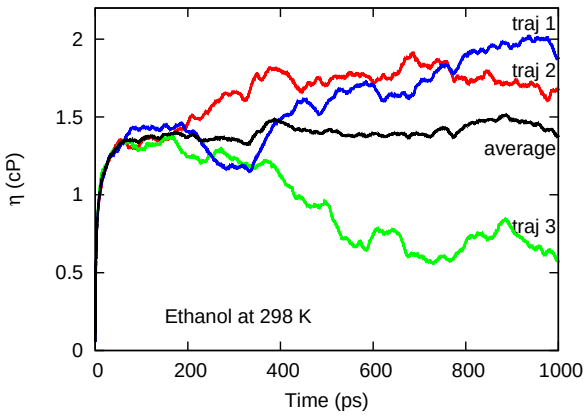
traj 1
traj 2
average
traj 3
Ethanol at 298 K
η (cP)
Time (ps)
0
0.5
1
1.5
2
0
200
400
600
800
1000

Figure 1:

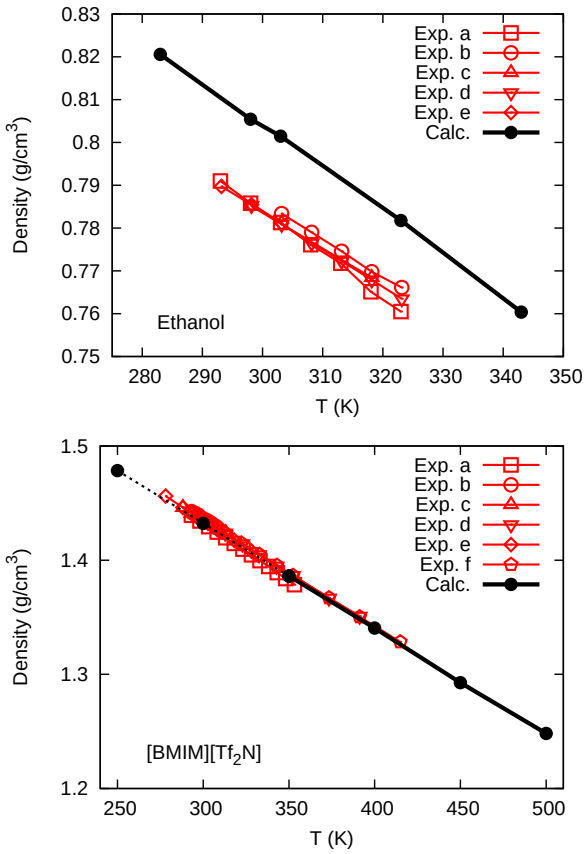
Density (g/cm^3)
T (K)
Exp. a
Exp. b
Exp. c
Exp. d
Exp. e
Calc.
Ethanol
Density (g/cm^3)
T (K)
Exp. a
Exp. b
Exp. c
Exp. d
Exp. e
Exp. f
Calc.
[BMIM][Tf$_2$N]

Figure 2:

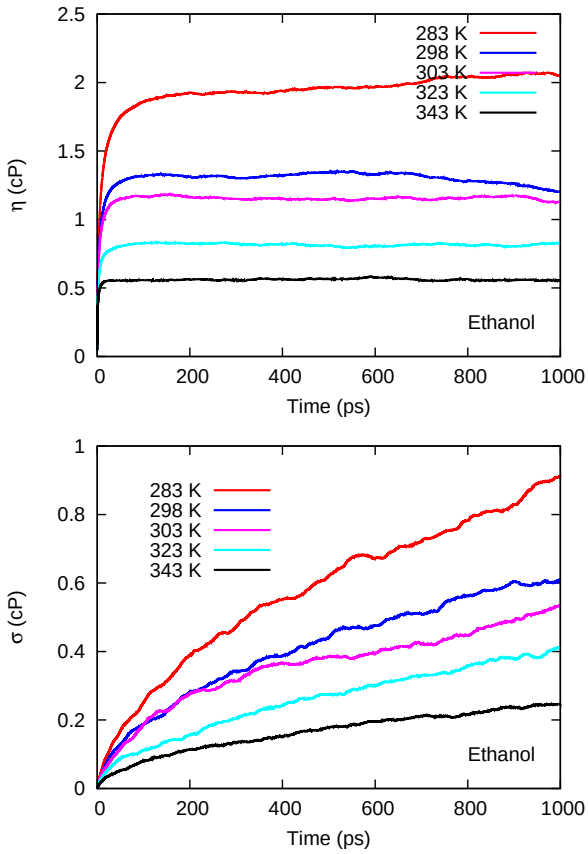
2.5
2
1.5
1
0.5
0
η (cP)
283 K
298 K
303 K
323 K
343 K
Ethanol
0
200
400
600
800
1000
Time (ps)
1
0.8
0.6
0.4
0.2
0
σ (cP)
283 K
298 K
303 K
323 K
343 K
Ethanol
0
200
400
600
800
1000
Time (ps)

Figure 3:

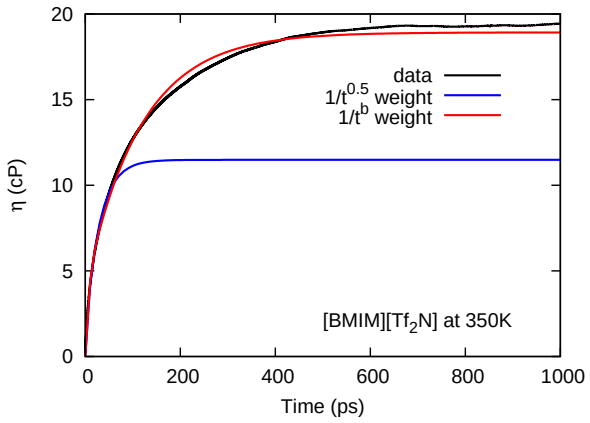
20
15
10
5
0
η (cP)
0
200
400
600
800
1000
Time (ps)
data
1/t^0.5 weight
1/t^b weight
[BMIM][Tf2N] at 350K

Figure 4:

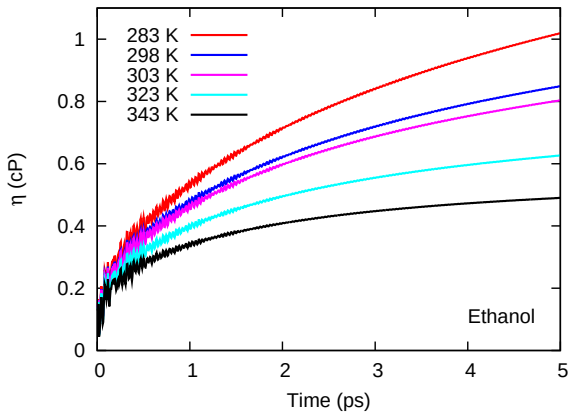
283 K
298 K
303 K
323 K
343 K
Ethanol
η (cP)
Time (ps)
0
0.2
0.4
0.6
0.8
1
0
1
2
3
4
5

Figure 5:

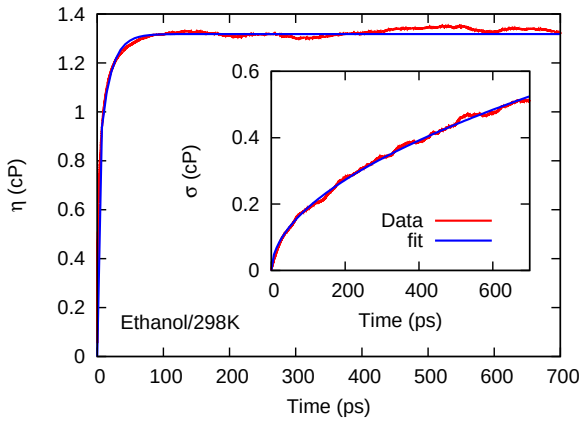

Figure 6:

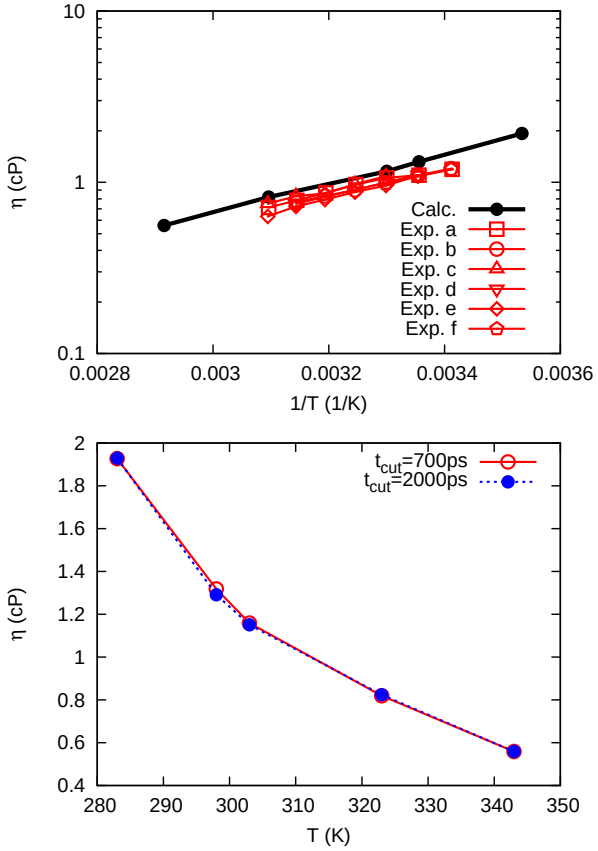
10
1
0.1
η (cP)
0.0028
0.003
0.0032
0.0034
0.0036
1/T (1/K)
Calc.
Exp. a
Exp. b
Exp. c
Exp. d
Exp. e
Exp. f
2
1.8
1.6
1.4
1.2
1
0.8
0.6
0.4
η (cP)
280
290
300
310
320
330
340
350
T (K)
tcut=700ps
tcut=2000ps

Figure 7:

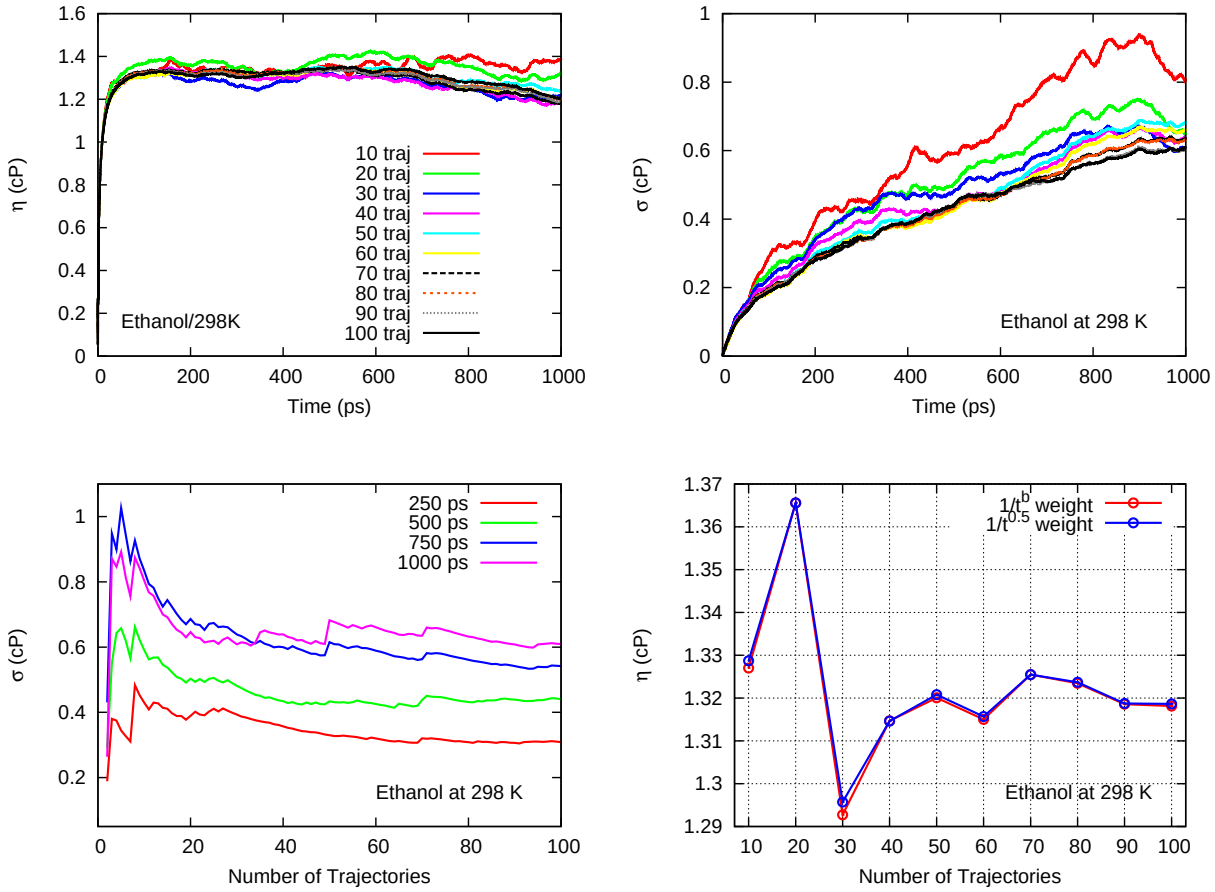
η (cP)
Time (ps)
Ethanol/298K
10 traj
20 traj
30 traj
40 traj
50 traj
60 traj
70 traj
80 traj
90 traj
100 traj
σ (cP)
Time (ps)
Ethanol at 298 K
σ (cP)
Number of Trajectories
250 ps
500 ps
750 ps
1000 ps
Ethanol at 298 K
η (cP)
Number of Trajectories
1/t^b weight
1/t^0.5 weight
Ethanol at 298 K

Figure 8:

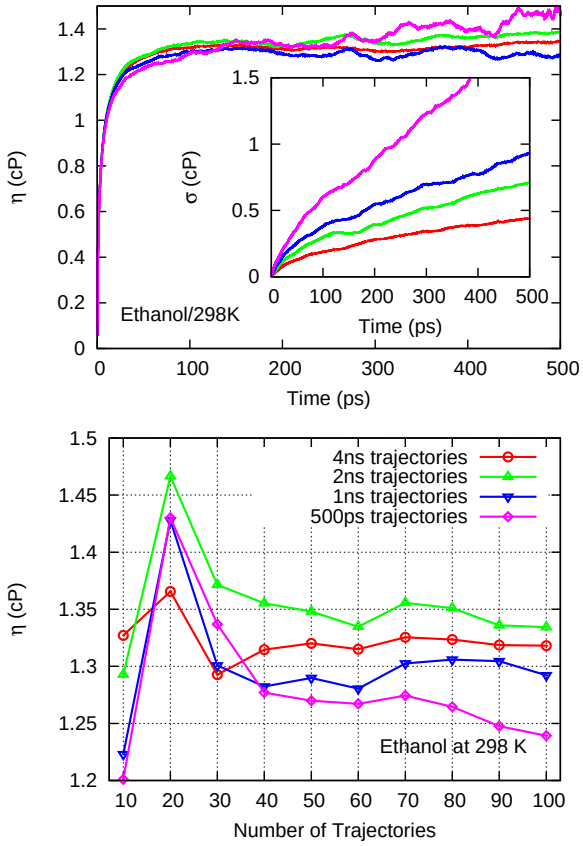
η (cP)
Time (ps)
Ethanol/298K
σ (cP)
Time (ps)
4ns trajectories
2ns trajectories
1ns trajectories
500ps trajectories
Ethanol at 298 K
η (cP)
Number of Trajectories

Figure 9:

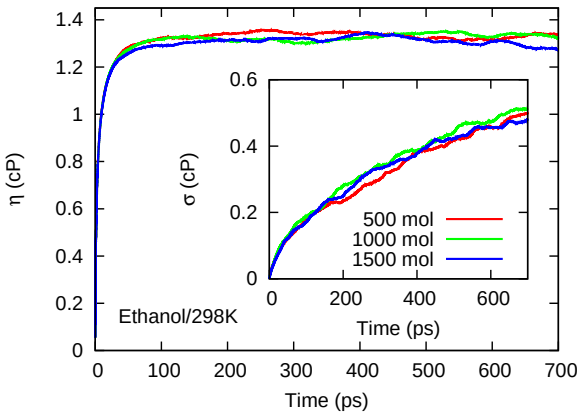
1.4
1.2
1
0.8
0.6
0.4
0.2
0
η (cP)
0
100
200
300
400
500
600
700
Time (ps)
Ethanol/298K
0.6
0.4
0.2
0
σ (cP)
0
200
400
600
Time (ps)
500 mol
1000 mol
1500 mol

Figure 10:

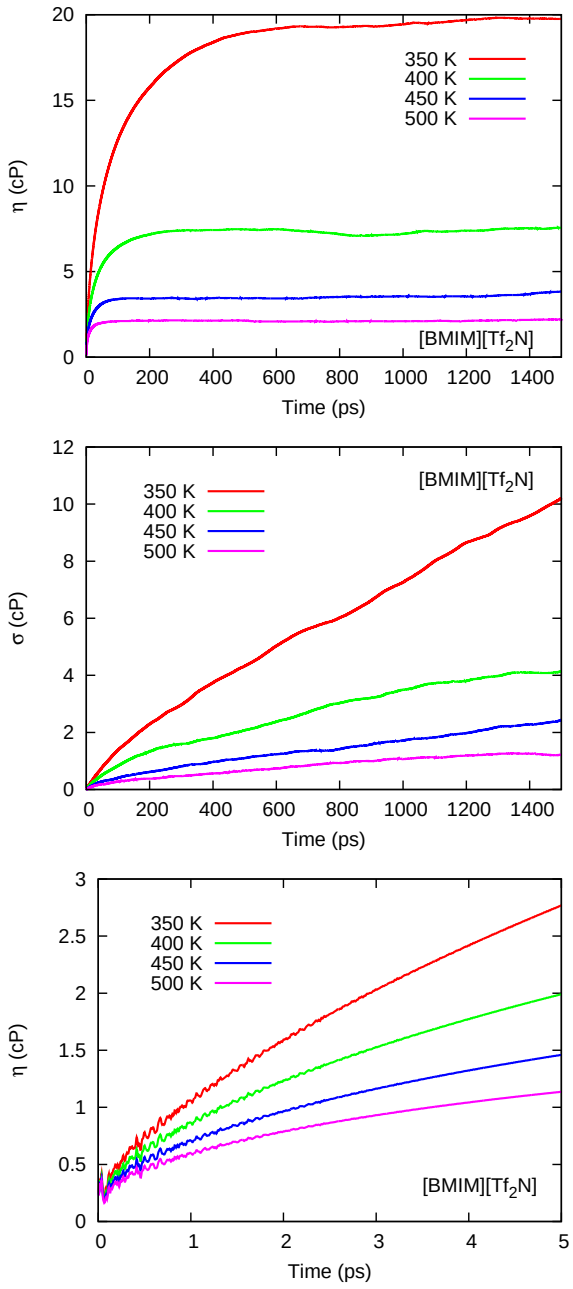
η (cP)
Time (ps)
350 K
400 K
450 K
500 K
[BMIM][Tf2N]
σ (cP)
Time (ps)
350 K
400 K
450 K
500 K
[BMIM][Tf2N]
η (cP)
Time (ps)
350 K
400 K
450 K
500 K
[BMIM][Tf2N]

Figure 11:

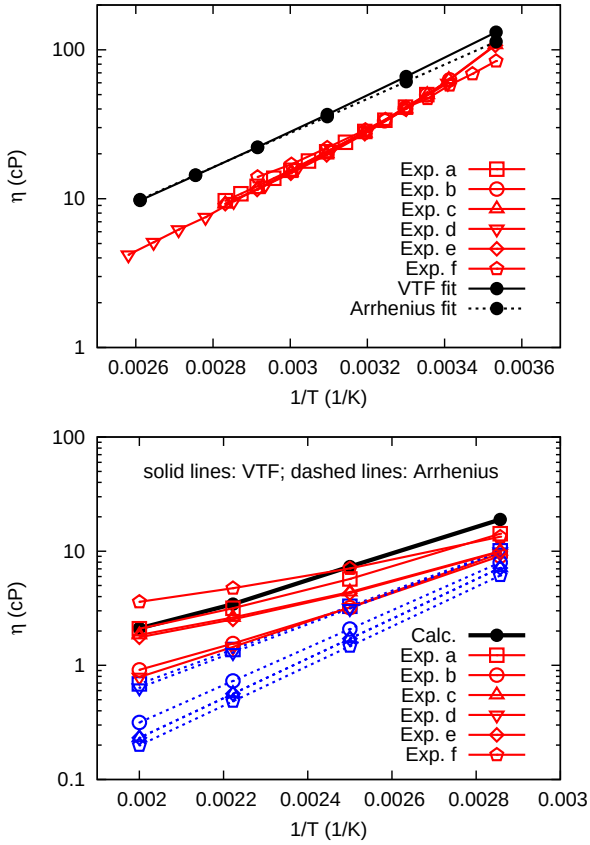
100
10
1
η (cP)
0.0026
0.0028
0.003
0.0032
0.0034
0.0036
1/T (1/K)
Exp. a
Exp. b
Exp. c
Exp. d
Exp. e
Exp. f
VTF fit
Arrhenius fit
100
10
1
0.1
η (cP)
solid lines: VTF; dashed lines: Arrhenius
0.002
0.0022
0.0024
0.0026
0.0028
0.003
1/T (1/K)
Calc.
Exp. a
Exp. b
Exp. c
Exp. d
Exp. e
Exp. f

Figure 12:

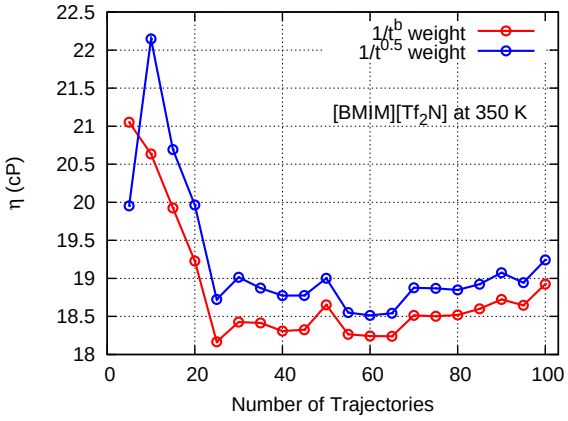
22.5
22
21.5
21
20.5
20
19.5
19
18.5
18
η (cP)
0
20
40
60
80
100
Number of Trajectories
1/t^b weight
1/t^0.5 weight
[BMIM][Tf2N] at 350 K

Figure 13: